Iraqi Journal of Physics, 2024 *Vol. 22, No. 2, PP. 116-126*
https://doi.org/10.30723/ijp.v22i2.1144 *P-ISSN: 2070-4003*
E-ISSN: 2664-5548

Green Synthesis of AgNPs and Fe_2O_3NPs Using Garlic Plant and Study their Anticancer Activity against Cervical Cancer Cells

Hala H. Ali[1a]* and Farah T. Mohammed Noori[1b]
[1]*Department of Physics, College of Science, University of Baghdad, Baghdad, Iraq*
E-mail: farah.noori@sc.uobaghdad.edu.iq
[a*]Corresponding author: hala.hussein1104a@sc.uobaghdad.edu.iq

Abstract

In this study, silver and iron nanoparticles were biosynthesized using the garlic plant, an economical and environmentally friendly method. A blend of chitosan (CS) and polyvinylalcohol (PVA) was prepared. The silver nanoparticles (AgNPs), iron oxide nanoparticles (Fe_2O_3NPs), and the (CS/PVA) blend were characterized by X-ray diffraction (XRD), Fourier-transform infrared spectroscopy (FTIR), and Field Emission Scanning Electron Microscopy (FE-SEM) analyses. The FE-SEM images revealed that Fe_2O_3NPs were cubical and hexagonal, and AgNPs were spherical aggregates. AgNPs with blend (CS/PVA) and Fe_2O_3NPs with blend (CS/PVA) and (Fe_2O_3NPs/blend (CS/PVA) /AgNPs) composite were synthesized and tested for anticancer activity against cervical cancer cells (Hela) using the MTT assay. Best kills and the highest inhibitory effect were observed in (AgNPs/ blend (CS/PVA)) and (Fe_2O_3NPs/blend (CS/PVA)/AgNPs) composite. These findings demonstrated the method's ability to synthesize nanocomposites with desirable physical, chemical and biological properties. Therefore, these findings demonstrate the new antibacterial and robust cytotoxicity features of the nanocomposite material, which has promising medical applications.

Article Info.

Keywords:
Biosynthesis, Green Synthesis, Nanomaterials, Cervical Cancer (Hela), Cytotoxicity.

Article history:
Received: Jun. 10, 2023
Revised: Oct. 22, 2023
Accepted: Oct. 31, 2023
Published: Jun. 01, 2024

1. Introduction

Recently, nanomaterial have attracted the great interest of researchers because of their distinctive properties. They have been used in various scientific fields, including biomedical, environmental sciences, and engineering [1]. There has been an increase demand for nanoparticles, which has resulted from large-scale manufacturers employing high-energy processes and solvents. Nanoparticles (NPs) exhibit unique electrical, optical, chemical, and biological capabilities. Functional structured nanoparticles have attracted significant attention in the biomedical field thanks to their use as vehicles for the controlled delivery of different types of drugs [2, 3]. Nanotechnology is an advanced technique that deals with nanometer-sized samples. Nano-materials are tiny, solid particles with sizes ranging between 1 and 100 nanometers, the therapeutic efficacy of NPs is strictly connected to their physicochemical properties such as size and morphology; however, to obtain NPs of the desired size and shape with high batch-to-batch reproducibility remains technically challenging in the conventional synthetic batch methods [4, 5], which is the key points for the treatment of many forms of cancer. In particular, NPs can increase the drug concentration in cancer cells and help to overcome some limitations of conventional chemotherapy such as the low specificity to cancer cells and the toxic effects on healthy cells [6, 7]. NPs can take advantage of the enhanced permeability and retention effect (EPR) that facilitates the NP accumulation into cells and tissues of solid tumors [8, 9]. The EPR effect is generally displayed by tumor vessels, which show some characteristics such as an anomalous rate of growth, a

disordered vascular architecture and high permeability [9]. Unfortunately, the EPR efficacy/efficiency is limited by some drawbacks such as a possible shortage of NPs cell uptake, an undesired release of the drug before the NPs are internalized and a low percentage of the administered dose [10]. A possible strategy to overcome these limitations is aimed at providing the NPs with active targeting moieties by means of appropriate modifications of NP surfaces such as nucleic acids [11, 12], antibodies [13], proteins [14] and folate [15]. Indeed, functionalized NPs can be recognized and subsequently bind to tumor cells and can even be internalized via receptor-mediated endocytosis [15, 16]. However not all modifications of the NP surface represent an effective strategy to overcome the limitations of EPR, for instance recently, folic acid-functionalized liposomes do not enhance the distribution of liposomes in FR-α-overexpressed tumors [17]. For all these reasons, the NP fabrication methods represent an important tool for the reproducibility of biological assays. In particular, there are a variety of NP synthetic conventional methods such as nano-precipitation [18], solvent evaporation [19, 20], micro-emulsions [21], sol–gel [22, 23], emulsion polymerization [24], layer-by-layer self-assembly [25], thin-film hydration [26], bulk mixing by extrusion [27], pipette mixing [28], electro deposition and thermal decomposition [29, 30]. In these methods, the formation of the NPs can be divided into three stages, a) nucleation, b) growth and c) aggregation, which occur concurrently leading to some differences, in terms of physicochemical properties, from batch-to-batch of synthesized NPs [31]. The inability to control the physicochemical properties of each synthetic batch of NPs leads to low reproducibility of both in vitro and consequently in vivo biological tests [32]. In particular, the nucleation, growth, and aggregation steps of the NPs can be separated as a function of distance from the position where the solution occurs in order to achieve absolute control of the physicochemical properties, including particle size and morphology [33, 34]. Thus, compared to conventional methods, the microfluidic technique overcomes all limitations for the production of NPs, increasing the reproducibility of each synthetic batch and favoring the industrial scale-up, and represents a new strategy capable of overcoming challenges in the clinical field of NP drug carriers [35].

In this study, we looked at how nanoparticles (Fe_2O_3NPs) and (AgNPs) affected Hela cell line. Cervical cancer is the fourth most prevalent disease in women worldwide and one of the top three malignancies affecting women under the age of (45y) [36-38]. Early-stage and locally invasive cervical cancer treatment options include eradication and combined chemotherapy and radiotherapy [39, 40]. Because of its potential to design useful systems, such as medicine delivery systems for humanity, nanotechnology has recently attracted a lot of attention [41]. Many efforts have been made to regulate the production of sub-nanometer particles and put it to use in the domains of physics, chemistry, biology, and even some areas of medicine [42]. Novel medication delivery systems based on nanoparticles have been developed to the application of nanotechnology; these systems have now contributed to precision medicine, they are being utilized in numerous therapeutic approaches, such as the targeted delivery of medications, prognostic visual monitoring of therapy, and even tumor identification [43]. Due to their capacity to target many bio-molecular characteristics among resistant strains, metal-NPs have been widely researched as a method to combat antibiotic resistance. FeNPs and AgNPs are two of the most common types of metal employed in the medical field [44]. These nanoparticles (FeNPs, AgNPs) can be synthesized using a wide range of physical and chemical techniques, including chemical reactions, photochemical processes, thermal degradation of different silver compounds, electrochemical processes, radiation, and microwave-assisted methods [45]. Some therapies use physical techniques, and others use chemical or biological techniques.

However, cost and efficiency are the key factors to consider when comparing various systems. Therefore, researchers looked for affordable and effective therapy options that wouldn't disturb the delicate balance of the environment [46]. The green method of biosynthesis for (silver and iron) nanoparticles has been This method is easy, clean, environmentally, friendly, and inexpensive as it gives samples in liquid form. These samples were used as a drug against cancer cells, specifically in this research against cervical cancer cells, to study the anticancer of cytotoxicity and autophagy inducer of cervical cancer (Hela cell line) [47].

This work objective is to study the effectiveness of AgNPs and Fe_2O_3NPs inducing killing in cancer cells (cervical). as cytotoxic and induction of autophagy. Autophagy is an intracellular degradation system that delivers cytoplasmic materials to the lysosome or vacuole. This system plays a crucial role in various physiological and pathological processes in living organisms ranging from yeast to mammals, wherein various cytoplasmic constituents are broken down and recycled through the lysosomal degradation pathway. This process consists of several sequential steps, including sequestration of cytoplasmic portions by isolation membrane to form autophagosome, fusion of the autophagosome with a lysosome to create an autolysosome, and degradation of the engulfed material to generate monomeric units such as amino acids by inhibition or killed. That helped to solve the global problem of different tumors [48].

2. Experimental Work

In this research, AgNPs and Fe_2O_3NPs were prepared biologically (Green synthesis) using garlic plant extract, and positive results were obtained. The garlic cloves were peeled and run under filtered water to remove any remaining debris and dirt. The aqueous extract was obtained by pounding 10 g of garlic with a pestle and mortar; this was combined with 100 ml of distilled water. The extract was filtered using filter paper, and the resulting filtrate was stored in the refrigerator at 4 °C for later use.

Nano-iron oxide and nano-silver were prepared using iron nitrate ($Fe(NO_3)_2$) and silver nitrate ($AgNO_3$), respectively, after mixing with garlic extract, diluted with distilled water, and adding it dropwise using a full pipet and 100 ml of 2 mg $AgNO_3$ and $Fe(NO_3)_2$. A magnetic stirrer at 650 revolutions per minute continually agitated the reaction mixture. After just a few seconds (less than 5 seconds), the colorless solution began to become white to dark brown, representing the creation of a silver colloid, and yellow to red-brown representing the creation of iron colloid, after 15 minutes, the color saturation reached a maximum. UV-Vis spectroscopy revealed the occurrence of this phenomenon at 380 nm for AgNPs and at 225 nm for Fe_2O_3NPs. The following tests (XRD, FTIR, and FE-SEM) confirmed the identity of the substance. The (CS/PVA) mixture was prepared by mixing 1 g of chitosan with 1 g of polyvinyl alcohol in 100 ml of distilled water in a beaker on a stirrer device with the use of a magnetic stirrer for continuous stirring at a constant speed to prevent agglomeration and burning; the temperature was fixed at 30^{o}C. The process lasted (2-2:30) hrs until a gelatinous liquid of a white to light yellow colour was obtained. Then the mixture was ready to be used. It was mixed with the prepared nanomaterials in certain proportions and pouring onto glass slides to obtain a sample in the form of a membrane so that it facilitates the process of conducting tests on it.

To calculate the cytotoxicity effect of Fe_2O_3NPs/blend (CS/PVA), AgNPs/blend (CS/PVA) and Fe_2O_3NPs/blend (CS/PVA)/AgNPs against (Hela) cells, a concentration of 104 HeLa cells in 100 microliters were cultured in DMEM and RPMI complete culture medium in a 96-well plate and incubated in an incubator at 37 °C.

Survival rate (%) and cytotoxicity rate (%) were calculated using the following equations:

survival rate (%)
= the average absorption of each sample
− the average absorption of nanoparticles
/the average absorption of the control) x 100 (**1**)

cytotoxicity rate (%) = 100 − Survival rate (**2**)

This method is easy, clean, environmentally, friendly, and inexpensive as it gives samples in liquid form. These samples were used as a drug against cancer cells, specifically in this research against cervical cancer cells, to study the anticancer of cytotoxicity and autophagy inducer of cervical cancer (Hela cell line).

3. Results and Discussion

The results of this study were compared to that of previous publications [47, 49, 50]. X-ray diffraction (XRD) analysis confirmed the crystalline form of the biosynthesized AgNPs by revealing four emission peaks at 2θ= 32.10°, 38.34°, 45.68°, and 77.59°, which correspond to the Miller indices (111), (200), (220), and (311) surfaces of silver [50], as shown in Fig. 1

The XRD pattern of the Fe_2O_3NPs is shown in Fig. 1. The characteristic diffraction is that there were three peaks arising at 2θ= 31.14°, 35.38° and 43.89°. They are respectively belonging to Miller indices (220), (311), and (400). [51], These distinctive peaks, which correspond to face-centered cubic (f.c.c.) symmetry, are consistent with reference diffraction data JCPDS: 39-1346 .

As for the blend (CS+PVA), the XRD analysis was random because it is an organic polymer. According to these findings, chitosan exhibits good compatibility, which promotes the development of a porous xerogel network. The mixed (CS/PVA) exhibits an amorphous form, which may be involved in biomedical applications, according to the XRD pattern. The mix of (Fe_2O_3NPs/blend (CS+PVA)/AgNPs) shows some peaks for AgNPs and Fe_2O_3NPs.

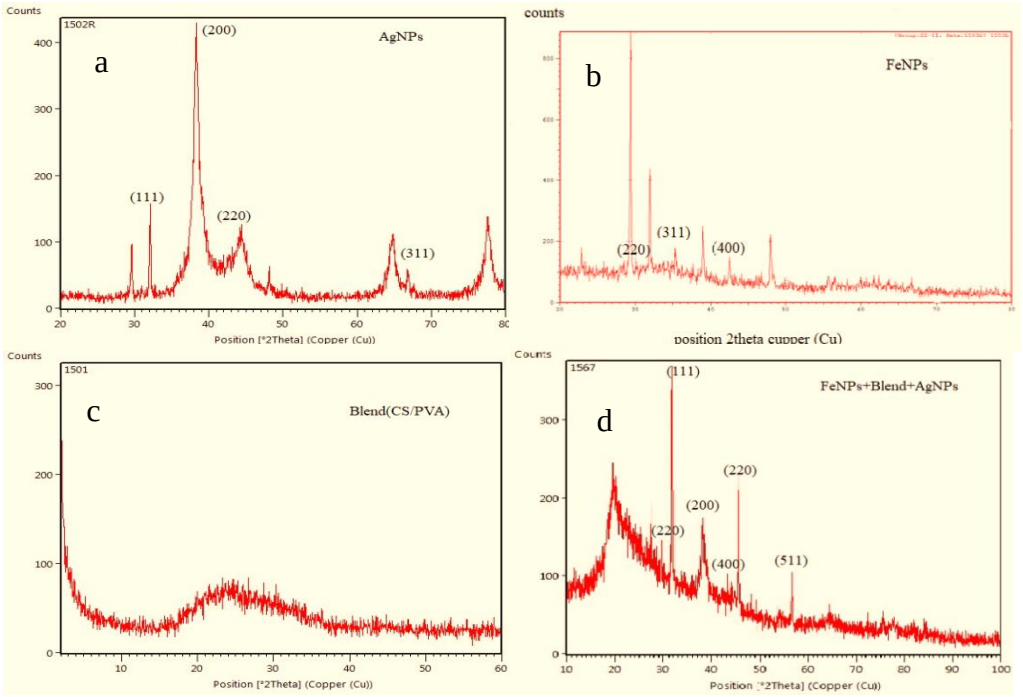

Figure 1: XRD for (a)AgNPs, (b)Fe_2O_3NPs, (c)Blend(CS/PVA) and (d)Fe_2O_3NPs /blend (CS/PVA)/AgNPs.

The FTIR spectra of biosynthesized AgNPs, as shown in Fig. 2a, showed peaks at 3418, 2916, 1602, 1384, 1111, 1057, 1031, and 602 cm^{-1}, which could be assigned to specific functional groups. For instance, the NH stretching of amide A was identified as the source of the peak at 3418 cm^{-1}. The peak at 2916 cm^{-1} represents the CH range of the alkanes. The carbonyl stretching vibration is indicated by the peak at 1602cm^{-1}. Carbohydrates' C-C-H, O-C-H, and C-O-H bending vibrational modes were all represented by the peaks at 1384, 1111 cm^{-1}, respectively. It has been suggested that the peaks at 1075, 1031 and 602 cm^{-1} are due to the (C-O) of an alkoxy group and CH_2 groups, respectively [50] Fig. 2.

In this investigation, FTIR was used to gain a better understanding of the biosynthesized Fe_2O_3NPs, as shown in Fig. 2b. The functional groups of the produced Fe_2O_3NPs were identified based on the FTIR analysis. FTIR spectra of biosynthesized Fe_2O_3NPs showed 13 peaks: at 3405, 2933, 2426, 1666, 1595, 1384, 1134, 1057, 1027, 938, 880, 835, and 602 cm^{-1}. The peak at 3405 cm^{-1}denotes alcohol OH, while the peaks at 2933, 2426, and 1666 cm^{-1} represent -H-C-H- and C=O stretching, respectively. The amide group and the -CN- stretching amine are responsible for the 1595 cm^{-1} and 1384 cm^{-1} peaks, respectively; the C-O stretch contributes to the 1134,1057, and 1027 cm^{-1} peak [50]. The biosynthesized blend was further characterized and the functional groups were identified based on the analysis of FTIR in this study. Indeed, many peaks at 3416, 2873, 1650, 1598, 1419, 1382, 1319, 1266, 1154, 1086, 1029, 898, 665 and 607 cm^{-1}, Fig. 2c shows a typical spectrum of blend (CS/PVA) film. The broad band at 3416 cm^{-1} is due to the OH stretching. The band at 1598 cm^{-1} is assigned to NH bending (amide II) (NH2) while the small peak at 1650 cm^{-1} is attributed to the C=O stretching (amide I) O=CNHR. The bands at 2873, 1419, and 1266 cm^{-1} are assigned to CH_2 bending due to pyranose ring 27 the band at 1382 cm^{-1} is due to CH_3 wagging. There is no noticeable change in Fe_2O_3NPs/blend (CS/PVA)/AgNPs because the preparation is composite and the reaction is not chemical.

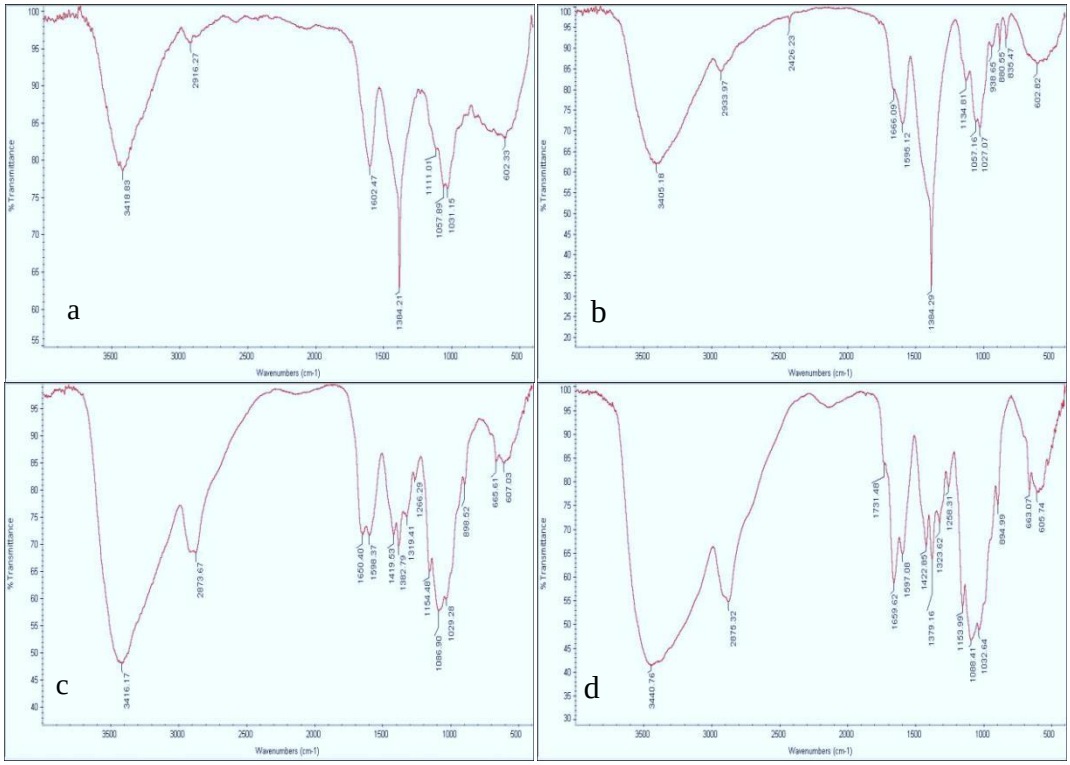

Figure 2: FTIR for (a) AgNPs, (b)Fe_2O_3NPs, (c)blend(CS/PVA) and (d)Fe_2O_3NPs/blend (CS/PVA)/AgNPs

Fig. 3 shows FE-SEM micrographs of AgNPs, Fe_2O_3NPs, and the blend (CS+PVA) at various magnifications, revealing that the AgNPs aggregated into spherical shapes with particle size D=23.21 nm, whilst the Fe_2O_3NPs were seen to be cubical, hexagonal, brick-like, and irregular in appearance with particle size D=22.39 nm. Fig. 3 demonstrates that the chitosan film has a rather smooth and homogenous surface with some straps, proving the excellent compatibility between chitosan and PVA. Hydrogen bonding between the functional groups of the blend component (CS+PVA) was primarily responsible for the development of homogenous blends of chitosan and PVA. EDX spectrum analysis contributes to a comprehensive understanding of the morphology and elemental composition of AgNPs, Fe_2O_3NPs, and the (CS/PVA) blend. These findings provide critical insights into these materials' physical properties and compatibility, which are essential for various applications in nanotechnology and material science.

Survival rate (%) and cytotoxicity rate (%) were calculated using Eqs. 1 and 2. Fig. 4 shows the cytotoxicity effect of Fe_2O_3NPs/blend (CS/PVA), AgNPs/blend (CS/PVA) and Fe_2O_3NPs/blend (CS/PVA)/ AgNPs against (Hela) cells, with concentration of 104 cells in 100 microliters of holes were cultured in DMEM and RPMI complete culture medium in a 96-well plate and incubated in an incubator at temperature of 37 °C. It was observed that the best results of kills were observed with AgNPs/blend (CS+PVA) and Fe_2O_3NPs/ blend (CS+PVA)/AgNPs, as shown in the Table 1.

Table 1: The viability and the cytotoxicity values of Fe_2O_3NPs/blend((CS/PVA), AgNPs/blend((CS/PVA) and Fe_2O_3NPs/blend((CS/PVA)/AgNPs for Cervical cancer cells.

Cervical Cancer				
Samples	**Control**	**Cell Viability**	**Control**	**Cell Cytotoxity**
AgNPs/blend (CS/PVA) (nano 4)	100%	25.5828%	0%	74.4172%
Fe_2O_3NPs/blend (CS/PVA)(nano 5)	100%	93.9449%	0%	6.0551%
Fe_2O_3NPs/ blend (CS/PVA)/AgNPs (nano 8)	100%	28.6104%	0%	71.3896%

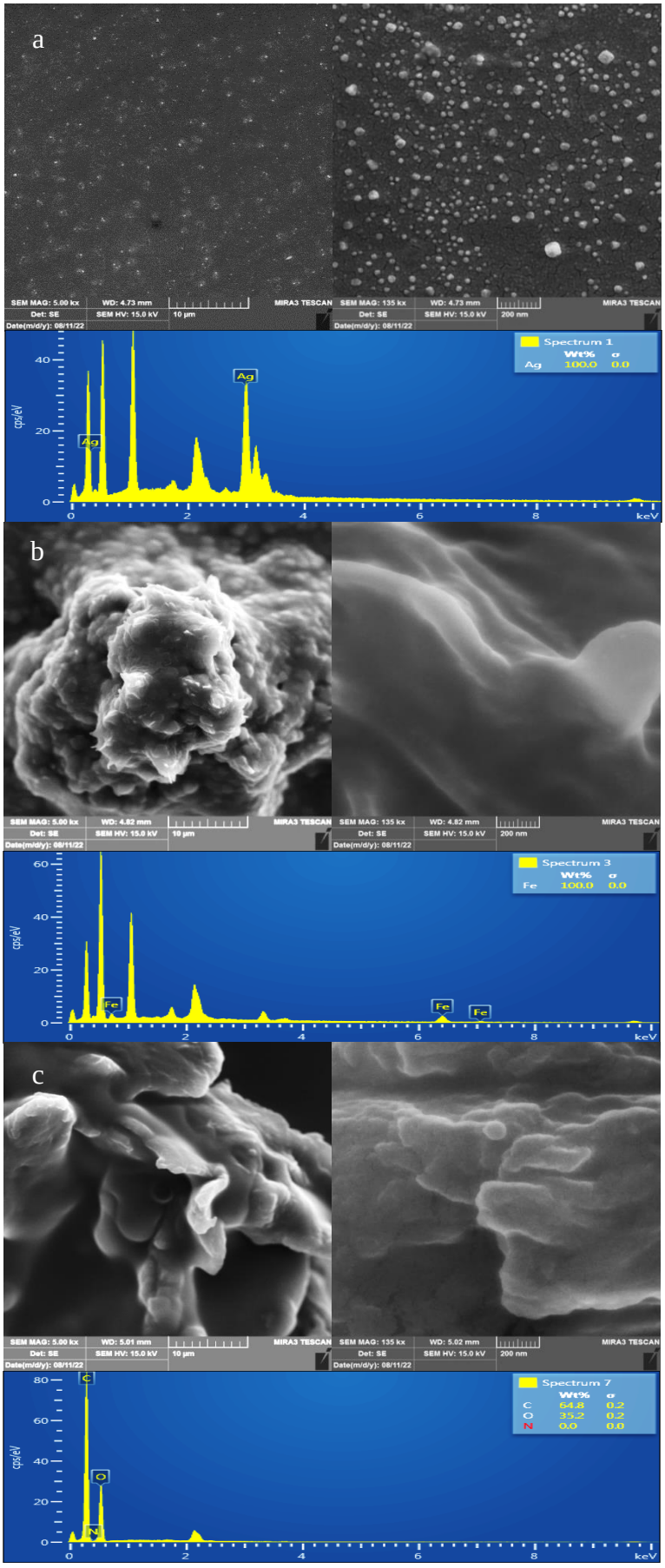

Figure 3: FE-SEM and EDX images of (a) AgNPs ,(b) Fe_2O_3NPs and(c) blend (CS/PVA).

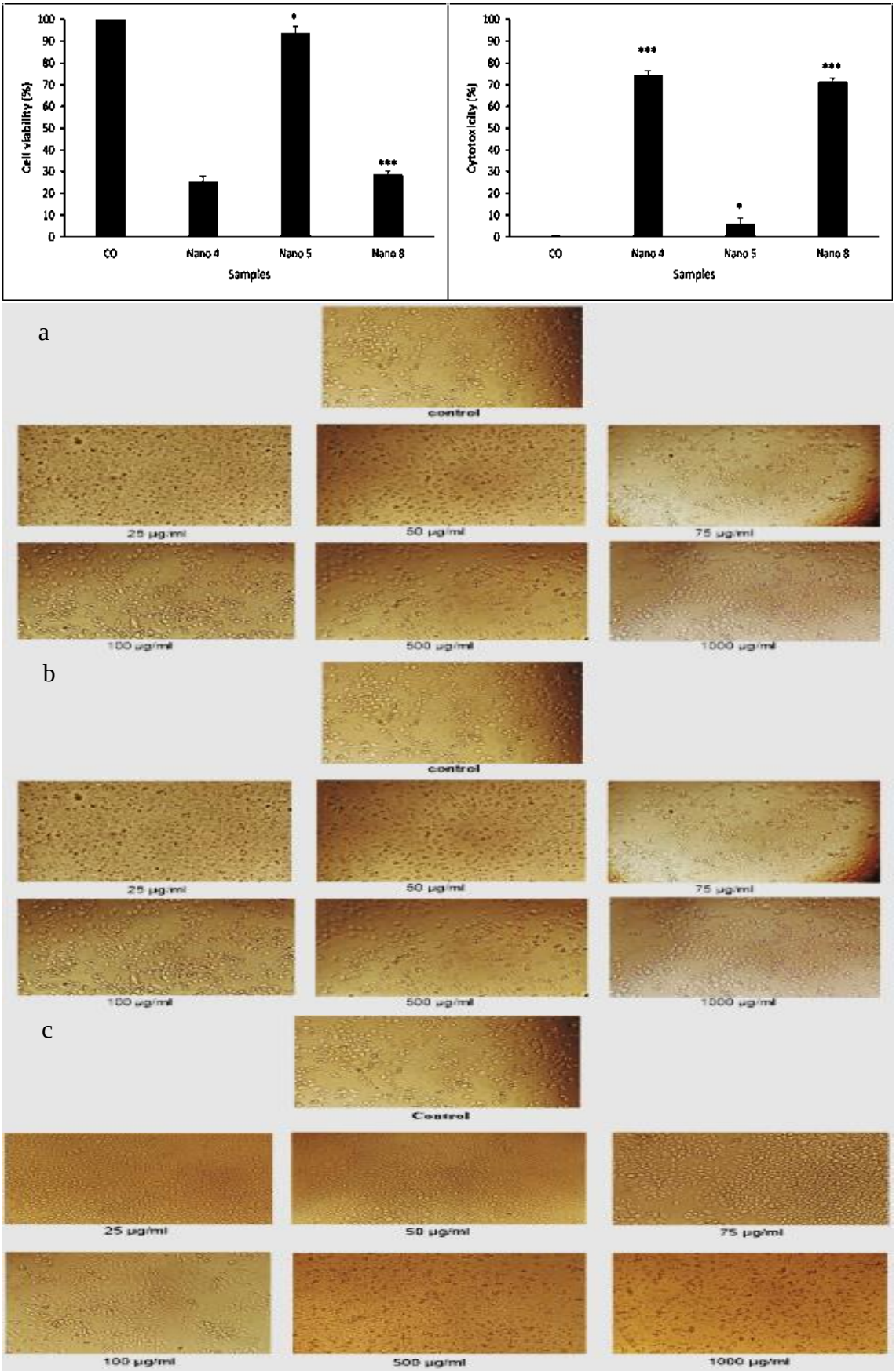

Figure 4: The viability and the cytotoxicity effect of (a)Fe_2O_3NPs/blend (CS+PVA), (b)AgNPs/blend (CS/PVA) and (c)Fe_2O_3NPs/blend (CS/PVA)/AgNPs for cervical cancer cell.

4. Conclusions

All the studies done on Fe_2O_3NPs and AgNPs have been successful for anti-cancers, exhibiting positive results in cervical cancer cells. Our work concludes that the cytotoxicity results obtained from MTT assay for Fe_2O_3NPs/ blend (CS/PVA) was 6.0551, for AgNPs/blend (CS/PVA) was 74.4172 and for Fe_2O_3NPs/blend (CS/PVA)/ AgNPs was 71.3896, especially the best results in the mixture that did exhibit powerful biological activities with biocompatibility and non-toxicity so the suitability of Ag and Fe in combination as metals for synthesis by garlic, and using it as composites with chitosan polymer by using biological method gave us very good results. However, more studies are needed in the in vitro, in vivo, and clinical domains to prove the usefulness of nanomaterials for their biological activities, as studies undertaken over the years have had significant limitations.

Acknowledgments

The authors would like to thank the University of Baghdad, College of Science, Department of Physics, for assisting us in this article.

Conflict of interest

The authors declare that they have no conflict of interest.

References

1. H. F. Al-Rubai, A. K. H. Al-Dahan, and B. A. Jasim, Iraqi J. Sci. **64**, 1592 (2023).
2. H. H. Abbas and S. N. Mazhir, Iraqi J. Phys. **21**, 9 (2023).
3. M. J. Mitchell, M. M. Billingsley, R. M. Haley, M. E. Wechsler, N. A. Peppas, and R. Langer, Nat. Rev. Drug Discov. **20**, 101 (2021).
4. A. Bokare, A. Takami, J. H. Kim, A. Dong, A. Chen, R. Valerio, S. Gunn, and F. Erogbogbo, ACS Omega **4**, 4650 (2019).
5. E. a. A. Kareem, A. E. Sultan, and H. M. Oraibi, Ibn AL-Haitham J. Pur. Appl. Sci. **36**, 177 (2023).
6. K. Cho, X. Wang, S. Nie, Z. Chen, and D. M. Shin, Clin. Canc. Res. **14**, 1310 (2008).
7. M. S. Ricci and W.-X. Zong, The Oncologist **11**, 342 (2006).
8. K. H. Bae, H. J. Chung, and T. G. Park, Molec. Cells. **31**, 295 (2011).
9. J. Wang, D. Mongayt, and V. P. Torchilin, J. Drug Targ. **13**, 73 (2005).
10. K. Y. Choi, H. Chung, K. H. Min, H. Y. Yoon, K. Kim, J. H. Park, I. C. Kwon, and S. Y. Jeong, Biomaterials **31**, 106 (2010).
11. E. Blanco, A. Hsiao, A. P. Mann, M. G. Landry, F. Meric-Bernstam, and M. Ferrari, Cancer Sci. **102**, 1247 (2011).
12. O. C. Farokhzad, J. Cheng, B. A. Teply, I. Sherifi, S. Jon, P. W. Kantoff, J. P. Richie, and R. Langer, Proce. Nat, Acad. Sci. **103**, 6315 (2006).
13. A. N. Lukyanov, T. A. Elbayoumi, A. R. Chakilam, and V. P. Torchilin, J. Cont. Rel. **100**, 135 (2004).
14. S. S. Aleksenko, A. Y. Shmykov, S. Oszwałdowski, and A. R. Timerbaev, Metallomics **4**, 1141 (2012).
15. J. D. Byrne, T. Betancourt, and L. Brannon-Peppas, Adv. Drug Deliv. Rev. **60**, 1615 (2008).
16. V. P. Torchilin, Advan. Drug Deliv. Rev. **58**, 1532 (2006).
17. H. Wang, T. Ding, J. Guan, X. Liu, J. Wang, P. Jin, S. Hou, W. Lu, J. Qian, and W. Wang, ACS Nano **14**, 14779 (2020).
18. K. H. Lee, G. Yang, B. E. Wyslouzil, and J. O. Winter, ACS Appl. Poly. Mat. **1**, 691 (2019).

19. Y. Liu, G. Yang, D. Zou, Y. Hui, K. Nigam, A. P. Middelberg, and C.-X. Zhao, Indus. Eng. Chem. Res. **59**, 4134 (2019).
20. N. Pinkerton, L. Behar, K. Hadri, B. Amouroux, C. Mingotaud, D. Talham, S. Chassaing, and J.-D. Marty, Nanoscale **9**, 1403 (2017).
21. X. Cui, J. Wang, X. Zhang, Q. Wang, M. Song, and J. Chai, Langmuir **35**, 9255 (2019).
22. S. Maiz-Fernández, L. Pérez-Álvarez, L. Ruiz-Rubio, R. Pérez González, V. Sáez-Martínez, J. Ruiz Pérez, and J. L. Vilas-Vilela, Polymers **11**, 742 (2019).
23. S. Y. Lee, E.-H. Hong, J. Y. Jeong, J. Cho, J.-H. Seo, H.-J. Ko, and H.-J. Cho, Biomat. Sci. **7**, 4624 (2019).
24. R. Wang, Y. Luo, S. Yang, J. Lin, D. Gao, Y. Zhao, J. Liu, X. Shi, and X. Wang, Sci. Rep. **6**, 33844 (2016).
25. J. Zhao, Z. Wan, C. Zhou, Q. Yang, J. Dong, X. Song, and T. Gong, Pharmac. Res. **35**, 1 (2018).
26. W. Wei, J. Sun, X.-Y. Guo, X. Chen, R. Wang, C. Qiu, H.-T. Zhang, W.-H. Pang, J.-C. Wang, and Q. Zhang, ACS Appl. Mat. Inter. **12**, 14839 (2020).
27. H. Patil, X. Feng, X. Ye, S. Majumdar, and M. A. Repka, AAPS J. **17**, 194 (2015).
28. D. Chen, K. T. Love, Y. Chen, A. A. Eltoukhy, C. Kastrup, G. Sahay, A. Jeon, Y. Dong, K. A. Whitehead, and D. G. Anderson, J. Amer. Chem. Soci. **134**, 6948 (2012).
29. R. Ciriminna, A. Fidalgo, V. Pandarus, F. Beland, L. M. Ilharco, and M. Pagliaro, Chem. Rev. **113**, 6592 (2013).
30. D. Desai, Y. A. Guerrero, V. Balachandran, A. Morton, L. Lyon, B. Larkin, and D. E. Solomon, Nanomedicine : nanotechnology, biology, and medicine **35**, 102402 (2021).
31. K. Zhai, X. Pei, C. Wang, Y. Deng, Y. Tan, Y. Bai, B. Zhang, K. Xu, and P. Wang, Int. J. Bio. Macromolec. **131**, 1032 (2019).
32. A. Fabozzi, F. Della Sala, M. Di Gennaro, N. Solimando, M. Pagliuca, and A. Borzacchiello, Poly. Chem. **12**, 6667 (2021).
33. T. Baby, Y. Liu, A. P. Middelberg, and C.-X. Zhao, Chem. Eng. Sci. **169**, 128 (2017).
34. J. Ma and C.-W. Li, Sens. Actuat. B Chem. **262**, 236 (2018).
35. D. R. Reyes, H. Van Heeren, S. Guha, L. Herbertson, A. P. Tzannis, J. Ducrée, H. Bissig, and H. Becker, Lab on a Chip **21**, 9 (2021).
36. M. Arbyn, E. Weiderpass, L. Bruni, S. De Sanjosé, M. Saraiya, J. Ferlay, and F. Bray, Lan. Glo. Heal. **8**, e191 (2020).
37. G. Bogani, F. Sopracordevole, V. Di Donato, A. Ciavattini, A. Ghelardi, S. Lopez, T. Simoncini, F. Plotti, J. Casarin, and M. Serati, Gyn. Oncol. **161**, 173 (2021).
38. M. Scioscia, M. Noventa, S. Palomba, and A. Laganà, BJOG: Int. J. Obst. Gyn. **128**, 2213 (2021).
39. C. Uwins, H. Patel, G. P. Bhandoria, S. Butler-Manuel, A. Tailor, P. Ellis, and J. Chatterjee, Clinic Onco. **33**, e372 (2021).
40. D. Cibula, R. Pötter, F. Planchamp, E. Avall-Lundqvist, D. Fischerova, C. Haie-Meder, C. Köhler, F. Landoni, S. Lax, and J. C. Lindegaard, Virch. Archiv **472**, 919 (2018).
41. V. Wagner, A. Dullaart, A.-K. Bock, and A. Zweck, Nat. Biotech. **24**, 1211 (2006).
42. A. J. Haider, A. L. Abed, and D. S. Ahmed, Iraqi J. Sci. **57**, 1203 (2016).
43. S. Sabeha and Z. J. Shanan, Ibn AL-Haitham J. Pur. Appl. Sci. **36**, 91 (2023).
44. G. M. Saleh, Iraqi J. Sci. **61**, 1289 (2020).
45. D. R. Ibraheem, N. N. Hussein, and G. M. Sulaiman, Iraqi J. Sci. **64**, 2223 (2023).

46. S. M. Abdullah, A. a. S. Al-Hamdani, and F. A. Resheed, Ibn AL-Haitham J. Pur. Appl. Sci. **36**, 201 (2023).
47. J. M. M. Mohamed, A. Alqahtani, T. V. A. Kumar, A. A. Fatease, T. Alqahtani, V. Krishnaraju, F. Ahmad, F. Menaa, A. Alamri, and R. Muthumani, Molecules **27**, 110 (2021).
48. S. N. Mizil, E. A. Elkaaby, and M. Z. Al-Shammary, bn AL-Haitham J. Pur. Appl. Sci. **36**, 60 (2023).
49. M. S. Samuel, S. Datta, N. Chandrasekar, R. Balaji, E. Selvarajan, and S. Vuppala, Nanomaterials **11**, 3290 (2021).
50. E. Ibrahim, M. Zhang, Y. Zhang, A. Hossain, W. Qiu, Y. Chen, Y. Wang, W. Wu, G. Sun, and B. Li, Nanomaterials **10**, 219 (2020).

التوليف الأخضر لـ AgNPs و Fe_2O_3NPs باستخدام نبات الثوم ودراسة نشاطها المضاد للسرطان ضد الخلايا السرطانية (عنق الرحم)

هالة حسين علي[1] وفرح طارق محمد نوري[1]
[1] قسم الفيزياء، كلية العلوم، جامعة بغداد، بغداد، العراق

الخلاصة

في هذه الدراسة تم تصنيع الجسيمات النانوية من الفضة والحديد حيوياً، وهي طريقة اقتصادية وصديقة للبيئة باستخدام نبات الثوم، بالإضافة إلى تحضير الخلطة (CS/PVA) باستخدام جهاز التحريك ذو المحرك المغناطيسي لغرض التحريك المستمر بسرعة ثابتة لمنع التكتل والاحتراق، حتى يتم الحصول على سائل هلامي ذو لون أبيض إلى أصفر فاتح وتم توصيف جزيئات الفضة النانوية (AgNPs) وجسيمات أكسيد الحديد النانوية (Fe_2O_3NPs) والخليط بواسطة حيود الأشعة السينية (XRD). أكد التحليل الطيفي للأشعة تحت الحمراء لتحويل فورييه (FTIR) والتحليل المجهري الإلكتروني لمسح الانبعاث الميداني (FE-SEM) .أوضحت صور FE-SEM أن Fe_2O_3NPs كانت مكعبة، سداسية، و AgNPs كانت مجاميع كروية. أيضا، تم اختبار المركبات المحضرة من أجل النشاط المضاد للسرطان ضد خلايا سرطان عنق الرحم (Hela) باستخدام مقايسة MTT، وأظهرت أفضل نتائج القتل وأعلى تأثير مثبط لوحظ في مركب (CS/PVA)) المركب بينما لوحظ (AgNPs/blend (CS/PVA)) في خطوط Hela الخلايا السرطانية من (Fe_2O_3NPs - مزيج (CS/PVA)) مركب (Fe_2O_3NPs / مزيج (AgNPs / (CS / PVA) أفضل النتائج وأعلى تأثير مثبط لخلايا سرطان عنق الرحم أيضًا، أظهرت هذه النتائج الطريقة القدرة على تصنيع مركبات النانو مع الخصائص الفيزيائية والكيميائية والبيولوجية المرغوبة. لذلك، توضح هذه النتائج الخصائص الجديدة المضادة للبكتيريا والسمية الخلوية القوية لمادة النانو المركب، والتي لها تطبيقات واعدة في الطب.

الكلمات المفتاحية: تخليق حيوي، التوليف الأخضر، المواد النانوية، سرطان عنق الرحم (هيلا)، السمية الخلوية.